DINAME 2023 - Proceedings of the XIX International Symposium on Dynamic Problems of Mechanics,
A.S. De Paula, A.T. Fabro and M.R. Machado (Editors), ABCM.
Pirenópolis, Go, Brazil, February 26th to March 3rd, 2023

Vibration Energy Harvesting using Shape Memory Alloys and Piezoelectric Materials

Arthur Adeodato[1], Luciana Loureiro S. Monteiro[1], Pedro Manuel C. L. Pacheco[1], and Marcelo A. Savi[2]

[1] CEFET/RJ, Department of Mechanical Engineering - Programa de Pós-Graduação em Engenharia Mecânica e Tecnologia de Materiais (PPEMM), Av. Maracanã, 229, 20271-110, Rio de Janeiro, RJ - Brazil.

[2] UFRJ - Universidade Federal do Rio de Janeiro, Center for Nonlinear Mechanics, COPPE – Department of Mechanical Engineering, P.O. Box 68.503, 21941-972, Rio de Janeiro, Brazil.

Abstract: Piezoelectric vibration energy harvesting has been receiving attention in scientific and industrial fields due to the ability to power supply sensors and devices through the direct piezoelectric effect. Since external conditions of excitation can vary through the harvesting process, there is a challenge to enhance energy harvesting capacity and adaptive systems are of special interest. This paper investigates the synergistic use of smart materials considering piezoelectric and shape memory alloy elements with the objective to enhance energy harvesting capacity. A constitutive model with polynomial phase transformation kinetics is used to describe the SMA thermomechanical behavior. Numerical simulations are carried out to evaluate the system response under different conditions. Results show that the special characteristics of shape memory alloys allow the energy harvesting system to operate over a wide frequency range.

Keywords: Vibration energy harvesting, piezoelectric materials, shape memory alloys, smart materials.

INTRODUCTION

New technological devices have an increasing dependence on energy sources, which are motivating new concepts of engineering projects where the energy must be harvested from the environment. This is even critical in situations with expensive or inappropriate access to the devices, including situations where the use of power cables is impracticable or with difficult battery replacements. That is the case of devices operating in remote areas as aeronautical (de Souza and de Marqui, 2015), oil wells (Lee et al., 2015), and biomedical applications including outside (Park et al., 2017) and inside (Dagdeviren et al., 2019; Ali et al., 2019) of living beings body.

Piezoelectric materials come up as an interesting alternative to power supply electronic devices in a way to avoid or reduce the use of power cables and battery components (Sodano et al., 2004a; Sodano et al., 2004b). Piezoelectricity is characterized by electromechanical coupling, being possible to be observed as the direct or reverse effects (Leo, 2007; Erturk and Inman, 2011). Therefore, the direct effect can be exploited to convert available environment mechanical energy into electrical energy that can be used to power devices or recharge batteries (Wiliams and Yates, 1996; Du Toit et al., 2005; Erturk, 2009).

Linear piezoelectric mechanical energy harvesting systems present a maximum energy conversion when the external frequency matches the resonant harvester condition. Nevertheless, since the ambient vibrations are unpredictable and can vary over a range of frequencies, linear piezoelectric energy harvesters present narrow bandwidth and operational range (Karadag and Topaloglu, 2018). The literature is vast about alternatives to enhance energy harvesting capacity and nonlinearities have shown to be the essential aspect (Tran et al., 2018). Nonlinearities allow to increase energy harvesting operational range, and can introduce adaptability and environment interaction. The synergistic use of smart materials is an innovative field that allows the combination of different materials to exploit adaptive behavior (Adeodato et al., 2021). On this basis, shape memory alloys (SMAs) can be used together with piezoelectric material to build an adaptive energy harvester. SMAs present solid phase transformations induced by either stress or temperature (Lagoudas, 2008; Elahinia, 2016), which allow property changes that confer adaptive behavior (Savi, 2015).

This paper deals with the synergistic use of piezoelectric materials and shape memory alloys to enhance the energy harvesting capacity through a range of frequencies. The energy harvester considers a piezoelastic beam coupled to an SMA element. The influence of SMA phase transformation is investigated considering the system nonlinear dynamics, monitoring the energy harvesting capacity. Linear model describes the electromechanical behavior of the piezoelectric element while SMA thermomechanical behavior is described by a novel polynomial phase transformation kinetics constitutive model. A single degree of freedom system is employed to describe the energy harvester dynamics. Numerical simulations are carried out considering different scenarios.

MATHEMATICAL MODEL

The traditional piezoelectric energy harvester is a cantilever beam subjected to base-vibration excitation, which can be modeled as a single degree of freedom (SDOF) electromechanical oscillator. Figure 1(a) shows a physical model of a piezoelectric energy harvester coupled to an SMA helical spring while Fig.1(b) shows its SDOF representation with

discrete parameters. The SMA spring is in austenitic phase at room temperature when in a stress-free state. The device considers preload that can alter its initial state and therefore, phase transformation can be induced either by the preload or by the base excitation.

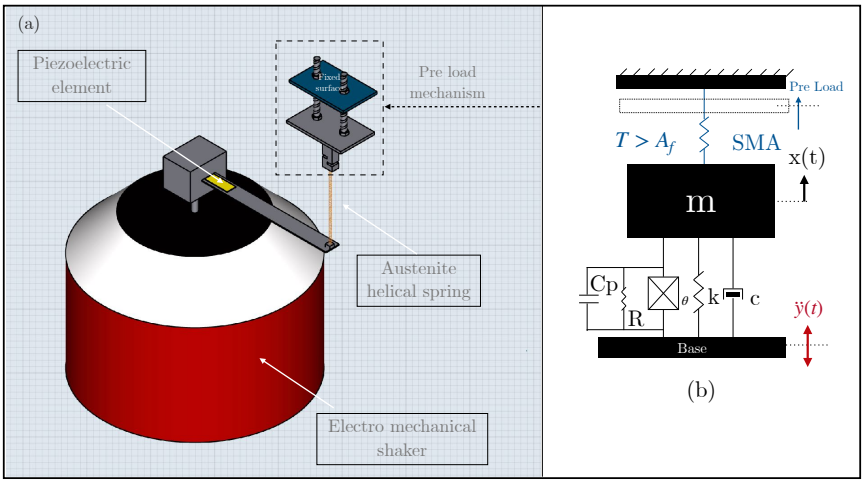

Figure 1 – SMA-piezoelectric energy harvester. (a) Physical model representing a piezoelastic beam connected with an SMA element and excited by a shaker. (b) Archetypal of a SDOF system.

The dynamical system can be described by two coupled differential equations representing the electromechanical system together with the constitutive model to describe the SMA behavior, represented by the term F_{SMA}:

$$m\ddot{z} + c\dot{z} + kz + F_{SMA} - \theta V = -m\ddot{y} \tag{1}$$

$$\theta z + C_p\dot{V} + \frac{V}{R} = 0 \tag{2}$$

where $y(t)$ is the base displacement, $z(t)$ is the relative displacement between base and body, and $V(t)$ is the electrical tension in the piezoelectric element. The harmonic base excitation is expressed by $\ddot{y} = A_b \sin(\Omega t)$ where A_b represents the maximum base vibration amplitude and Ω is the driven frequency; m represents the body mass, c is the linear viscous damping coefficient, and k is a linear stiffness associated with the restoring forces. θ, C_p, and R respectively represent the electromechanical coupling, circuit capacitance, and total load resistance for a closed-circuit condition.

The energy harvesting performance is monitored by considering input power P_{in} that is essentially the mechanical power: $P_{in} = m\ddot{y}\dot{z} = mA_b \sin(\Omega t)\dot{z}$; and the output power P_{out}, which is associated with the electrical power: $P_{out} = \frac{V^2}{R}$. System efficiency can be evaluated by considering the ratio between output and input power: $\eta = \frac{P_{out}}{P_{in}}$.

SMA Consitutive Model

The constitutive model to describe the SMA thermomechanical behavior is now in focus. A model with polynomial phase transformation kinetics is adopted (Adeodato et al., 2022), considering as state variables, the shear stress, τ, the shear strain, γ, the temperature, T, and the internal variable, β that represents martensitic volume fraction, where β_S is the stress induced detwinned martensite, and β_T is the temperature induced twinned martensite ($\beta = \beta_S + \beta_T$).

$$\dot{\tau} = G\dot{\gamma} + \alpha\dot{\beta} + \Theta\dot{T} \tag{3}$$

where G represents the shear modulus defined as $G = G_A + \beta(G_M - G_A)$. In addition, $\alpha = -G\gamma_R$ where γ_R is the residual strain, and Θ is the thermal expansion coefficient. The critical phase transformation stresses are defined as follows: $\tau_{Ms} = \tau_s + C_M(T - M_s)$, $\tau_{As} = C_A(T - A_s)$, $\tau_{Mf} = \tau_f + C_M(T - M_f)$ and $\tau_{Af} = C_A(T - A_f)$. In this regard, the martensitic volume fraction (β) can be expressed as follows:

$$\beta = \beta_0 + (1 - \beta_0) f_M(\tilde{\tau}_M, \tilde{T}_M) \quad A \to M \tag{4}$$

$$\beta = \beta_0 f_A(\tilde{\tau}_A, \tilde{T}_A) \quad M \to A \tag{5}$$

where the hardening functions $f_M(\tilde{\tau}_M, \tilde{T}_M)$ and $f_A(\tilde{\tau}_A, \tilde{T}_A)$ are expressed by two successive second order polynomial equations each and β is expressed as two consecutive second order polynomial equation. In addition, $\tilde{\tau}_M = \frac{\tau - \tau_{Ms}}{\tau_{Mf} - \tau_{Ms}}$, $\tilde{\tau}_A = \frac{\tau - \tau_{Af}}{\tau_{As} - \tau_{Af}}$, $\tilde{T}_M = \frac{T - M_s}{M_s - M_f}$ and $\tilde{T}_A = \frac{T - A_f}{A_s - A_f}$.

Regarding stress induced phase transformation, assumed to be at a constant temperature, the martensitic volume fraction can be reduced to $\beta = \beta_S$ and the hardening functions becomes $f_M(\tilde{\tau}_M)$ and $f_A(\tilde{\tau}_A)$, defined as follows:

$$f_M(\tilde{\tau}_M) = \begin{cases} a_1 \tilde{\tau}_M^2 + b_1 \tilde{\tau}_M + c_1 \\ a_2 \tilde{\tau}_M^2 + b_2 \tilde{\tau}_M + c_2 \end{cases} \tag{6}$$

$$f_A(\tilde{\tau}_A) = \begin{cases} a_3 \tilde{\tau}_A^2 + b_3 \tilde{\tau}_A + c_3 \\ a_4 \tilde{\tau}_A^2 + b_4 \tilde{\tau}_A + c_4 \end{cases} \tag{7}$$

where $0 < B_M < 1$ and $0 < B_A < 1$ are controlling parameters for forward and reverse transformations, respectively, defining start and finish of the polynomial curve. By solving the system for the boundary conditions, the polynomial coefficients are set as: $a_1 = 1/B_M$, $a_2 = 1/(B_M - 1)$, $b_2 = -2/(B_M - 1)$, $c_2 = B_M/(B_M - 1)$, $a_3 = 1/(B_A - 1)$, $b_3 = -2/(B_A - 1)$, $c_3 = -B_A/(B_A - 1)$, and $a_4 = 1/B_A$. This leads to the stress–strain relation for forward phase transformation as follows (Adeodato et al., 2022):

$$(\beta_0 - 1)\, a_1 \alpha \tilde{\tau}_M^2 + \tau - \alpha\beta_0 - \tau_0 - G\gamma + G_0\varepsilon_0 + \alpha_0\beta_0 = 0 \quad \text{if } 0 < \tilde{\tau}_M < B_\text{M} \tag{8}$$

$$(\beta_0 - 1)\, a_2 \alpha \tilde{\tau}_M^2 + (\beta_0 - 1)\, b_2 \alpha \tilde{\tau}_M + \tau - \alpha\beta_0 + (\beta_0 - 1)\, c_2 \alpha - \tau_0 - G\gamma + G_0\gamma_0 + \alpha_0\beta_0 = 0 \quad \text{if } B_\text{M} < \tilde{\tau}_M < 1 \tag{9}$$

$$-\beta_0 a_3 \alpha \tilde{\tau_A}^2 - \beta_0 b_3 \alpha \tilde{\tau}_A + \tau - \beta_0 c_3 \alpha - \tau_0 - G\gamma + G_0\gamma_0 + \alpha_0\beta_0 - \tau_0 - G\gamma + G_0\gamma_0 + \alpha_0\beta_0 = 0 \quad \text{if} \quad B_\text{A} < \tilde{\tau}_A < 1 \tag{10}$$

$$-\beta_0 a_4 \alpha \tilde{\tau}_A^2 + \tau - \tau_0 - G\gamma + G_0\gamma_0 + \alpha_0\beta_0 = 0 \quad \text{if } 0 < \tilde{\tau}_A < B_\text{A} \tag{11}$$

The energy harvester employs an SMA helical spring connected to the piezoelastic beam and therfore, it is necessary to model this element. By assuming plane section hypothesis, the torsional shear stress at the wire periphery (γ_p) and total elongation ($d_{SMA} = L - L_0$) can be written as:

$$d_{SMA} = \frac{\pi N D^2}{d} \gamma_p \tag{12}$$

By considering a linear strain distribution as a function of radial coordinate a, $\gamma = \frac{2a}{d}\gamma_p$ for $0 < a \leq d/2$, F_{SMA} becomes:

$$F_{SMA} = \frac{4\pi}{D} \int_0^r \tau(a) a^2 da \tag{13}$$

de Aguiar et al. (2010) and Enemark et al. (2014) discuss the main hypotheses for the modeling of SMA helical springs. On this basis, phase transformations are assumed to be uniform in the wire cross-section, considered to be associated with a constant strain $\gamma_{eq} = \frac{3}{4}\gamma_R$ and a constant equivalent stress $\tau_{eq} = G(\gamma_{eq} - \alpha\beta_{eq})$:

$$F_{SMA} = \frac{\pi d^3}{6D} \tau_{eq} \tag{14}$$

and substituting γ_{eq} into Eq. 12, it becomes:

$$d_{SMA} = \frac{4\pi N D^2}{3d} \gamma_{eq} \tag{15}$$

RESULTS AND DISCUSSION

This section investigates the influence of SMA on the piezoelectric energy harvester operation. Stress-induced phase transformations are of concern considering both preload and also by base vibration motion. Table 1 presents the parameters employed for the SDOF oscilaltor based on the experimental apparatus discussed in Adeodato et al. (2021).

Table 1 – Piezoelectric energy harvester discrete parameters.

m (kg)	k (N/m)	c (Ns/m)	θ (N/V)	R (kOhm)	C_p (F)
0.01	213	0.05	-3.1x10^{-5}	150	2.48x10^{-8}

A commercial SMA helical spring (Moreli Ortodontia) is used, presenting pseudoelastic effect at room temperature (298 K). The SMA spring presents a wire diameter d = 0.25 mm, helical diameter D = 1.25 mm, and 40 spires (N), and an initial length of 15 mm (L) free of stress. Experimental themomechanical characterization is performed considering DSC tests and quasi-static tensile tests that allow to build force-displacement curves using an Instron testing system (5966 model) with a controlled displacement rate of 4 mm/min. Tests are carried out at constant room temperature and different conditions of maximum prescribed displacement, following the procedures described in Adeodato et al. (2022). Table 2 shows the parameters for the SMA austenite helical spring.

Table 2 – *SMA* austenite helical spring experimental constitutive parameters.

M_s (K)	M_f (K)	A_s (K)	A_f (K)	
281.6	266.3	274.3	289.6	
G_A (GPa)	G_M (GPa)	C_A (MPa)	C_M (MPa)	γ_R
27.5	19.6	9	11	0.015

Force-displacement curves are built by considering the polynomial phase transformation model and results are shown in Figure 2 together with experimental curves. Figure 2 also shows the equivalent stress-strain diagrams.

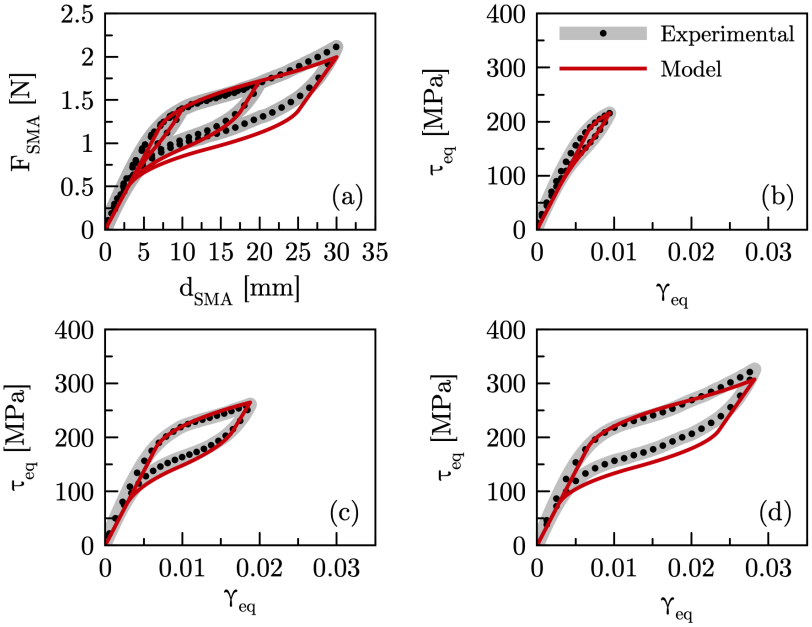

Figure 2 – SMA helical spring comparing polynomial phase transformation model and experimental data. (a) Force-displacement curve for different maximum load amplitude. Equivalent stress-strain curves for: (b) $\gamma_{max} = 0.01$**. (c)** $\gamma_{max} = 0.02$**. (d)** $\gamma_{max} = 0.03$

An analysis of preload value (PL) needs to be developed for the design of the energy harvester. The choice of PL = 1.5 N is related to a safe operation condition even for high levels of vibration base amplitude and do not exceed the quasi-static tested load levels. In this regard, PL = 0.5 N and PL = 1.0 N are also considered as intermediate values.

The influence of SMA preload in the energy harvester behavior is of concern considering a condition where base vibration is not able to promote significant phase transformation. Therefore, martensitic phase transformation remains basically restricted due to the quasi-static preloads. Figure 3 shows SMA piezoelectric energy harvester frequency response where curves are built considering up-sweep forcing frequency. The initial conditions are null at the beginning of the simulation. The base vibration amplitude (A_b) is set as 10 m/s^2 and different values of preload are treated, PL: 0, 0.5, 1 and 1.5 N. In addition, a case considering no phase transformation (without preload) is evaluated representing a linear piezoelectric harvester where SMA austenite helical spring assumes constant shear modulus ($G = G_A$). Maximum relative displacement, output power, input power, and efficiency are shown in Fig. 3(a), (b), (c), and (d), respectively, indicating that the preload is able to alter SMA spring stiffness and, as a consequence, shifts the resonance peak. Fig. 3(e) and (f) show the maximum equivalent shear stress and martensitic volume fraction in spring wire cross section. Note that the martensitic volume fraction is not significantly altered by the dynamical load. A dynamical jump is observed for the case where PL = 1.0 N.

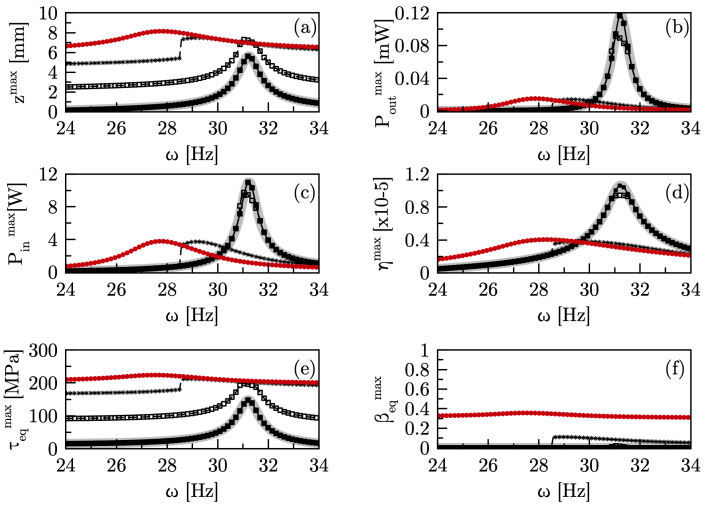

Figure 3 – Maximum values in frequency response analysis for A_b = 10 m/s^2. (a) Relative displacement. (b) Output power. (c) Input mechanical power. (d) Efficiency. (e) Equivalent SMA stress. (f) Equivalent SMA martensite volume fraction.

Figure 4(a) highlight the output power for A_b 10 m/s^2 and the curves distribution show an improvement in energy conversion for the case of PL = 1 N and PL = 1.5. It is noticeable a region between 26 to 28 Hz where the harvester can operate with more output power and efficiency than the other conditions. The case without preload (PL = 0 N) presents a response that matches the linear case. On the other hand, the case with PL = 1.5 N indicates a shift Δ_f = 3.34 Hz (31.19 - 27.85) in resonance peak when compared with PL = 0 N and the linear case, representing a difference of 10.7% from the initial natural frequency value (31.19 Hz).

Output power is also investigated in Fig. 4(b) by observing system performance at a stationary forcing frequency for ω = 27.85 Hz attributed to the resonance condition for PL = 1.5 N. Besides, comparing the linear case with the case of PL = 1.5 N, a total amount of Δ_{power} = 0.014 mW is observed indicating an increase around 15 times for the mentioned conditions.

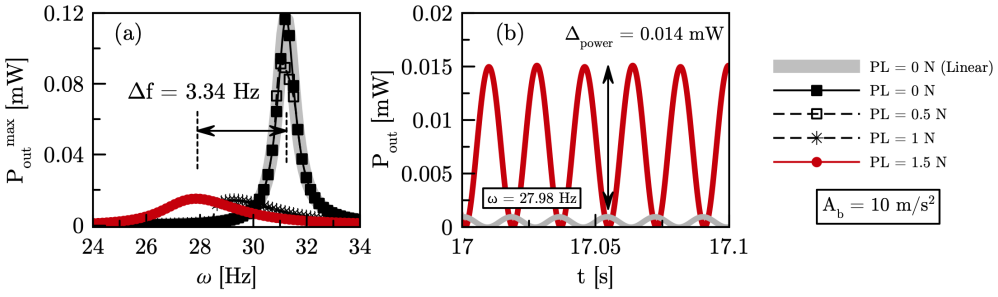

Figure 4 – Maximum output power frequency response analysis for A_b = 10m/s^2. (b) Output power comparison in steady state response for stationary forcing frequency ω = 27.98 Hz.

Figure 5 shows output power frequency response for A_b = 30 m/s^2 for some selected preload values (PL). Note that the increase of the phase transformation level promotes a shift on the resonance peak. It should also be noted that there is a region between 25 to 31 Hz where the change in SMA spring mechanical properties is able to increase the total output power and efficiency. Dynamical jumps are observed for some levels of phase transformation (PL = 0 and 0.5 N). A significant amount of martensitic volume fraction is obtained in the resonance region for A_b = 30 m/s^2.

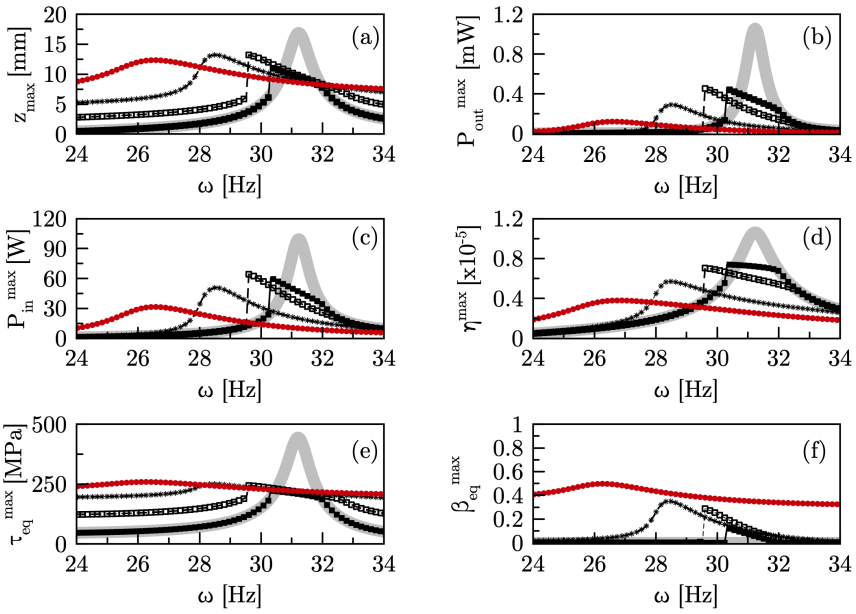

Figure 5 – Maximum values in frequency response analysis for A_b = 30 m/s^2. (a) Relative displacement. (b) Output power. (c) Input mechanical power. (d) Efficiency. (e) Equivalent SMA stress. (f) Equivalent SMA martensite volume fraction.

Following the same framework, the system operational range is evaluated by observing the output power frequency response in Fig. 6(a). The difference in resonance peak is evaluated enhancing the ability to shift the resonance frequency Δ_f = 4.62 (31.19 - 26.57) Hz. This value represents an increase of 14.81% with respect to the linear case and it is confirmed by the stationary forcing frequency steady state response as in Fig. 6(b).

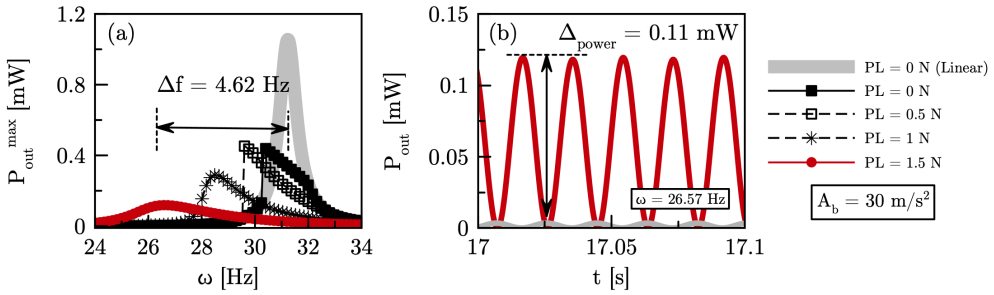

Figure 6 – Output power analysis. (a) Maximum output power frequency response for A_b = 30 m/s^2. (b) Output power comparison in steady state response for stationary forcing frequency ω = 26.67 Hz.

Figure 7 presents an investigation of stationary forcing frequency for ω = 26.57 Hz attributed to resonance peak for PL = 1.5 N and A_b = 30 m/s^2. Figure 7(a) and (b) shows relative displacement during preload, transient and steady state regimes. Again, the steady state response is rendered in red and highlighted in Fig. 7(c). Figure 7(d) shows force-displacement curve for SMA spring while Fig. 7(e) shows equivalent shear stress in SMA spring wire cross-section time evolution. The steady state response is highlighted in red. Figure 7(f) deals with equivalent martensitic volume fraction time evolution. The preload promotes an initial phase transformation and, in addition, base vibration motion promotes an oscillatory phase transformation. The dissipation capacity is considerably altered due to hysteresis loop. It is possible to note how the dynamical load provided by base vibration is able to influence equilibrium conditions by SMA phase transformation and changes the mechanical properties.

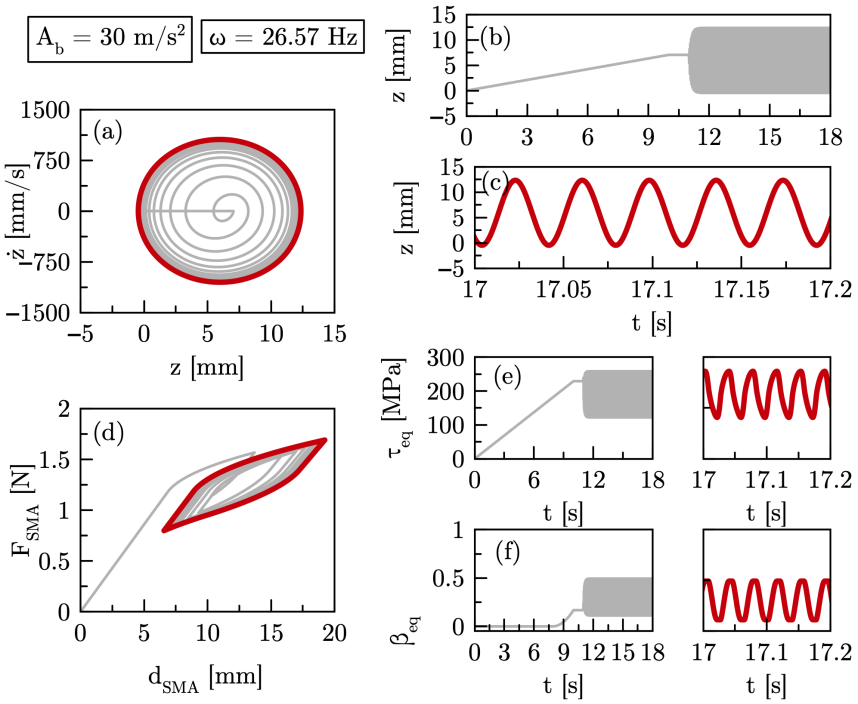

Figure 7 – Stationary forcing frequency analysis. (a) Phase space diagram. (b) Relative displacement time evolution. (c) Relative displacement steady state response. (d) SMA spring axial Force × displacement. (e) Equivalent shear Stress × Strain time evolution. (f) Equivalent martensite volume fraction time evolution

Figure 8 deals with $PL = 0.5N$, a situation where the maximum output power is reached, comparing the output power frequency response with the linear case for A_b = 30 m/s^2 which is associated with Δ_f = 1.59 Hz. Fig. 8(b)-(d) shows the force-displacement curve, phase space and output power for stationary forcing frequency ω = 29.6 Hz, respectively, while Fig. 8(e)-(g) for ω = 29.4 Hz. Fig. 8(a) indicates a dynamical jump and the system sensitivity for the forcing frequency parameter. Between ω = 29.4 and ω = 29.6 Hz, there is an increase around 100 times of the output power at steady state response (0.453 - 0.00426 mW).

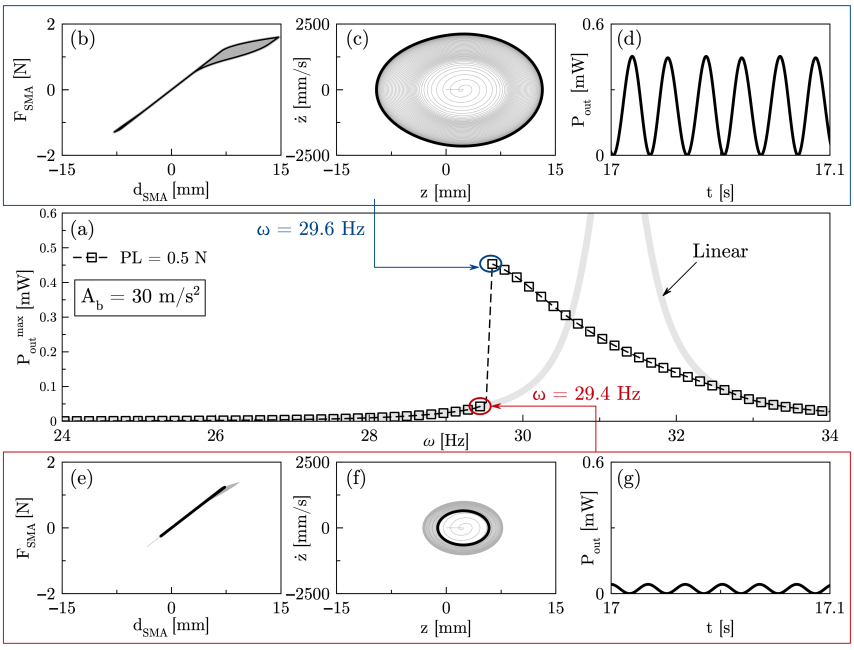

Figure 8 – Analysis of PL = 0.5 N. (a) Output power frequency response for A_b = 30 m/s^2. For stationary forcing frequency and ω = 29.6 Hz: (b) Force x Displacement, (c) phase space and (d) output power. For ω = 29.4 Hz, (e) Force x Displacement, (f) phase space and (g) output power.

CONCLUSIONS

The synergistic use of SMA and piezoelectric material is investigated for energy harvesting purposes. The effect of stress-induced phase transformation is of concern considering different preloads and base excitation. Numerical simulations show that phase transformations shift the harvester frequency response by around 15% of natural frequency. In addition, it is possible to estimate an increase of around 30 times at maximum output power in the case of a stationary forcing frequency where preload changes in order to tune the harvester on resonance condition. Overall, the adaptive characteristics of SMAs are interesting to enhance energy harvesting capacity of the classical piezoelectric systems.

ACKNOWLEDGMENTS

The authors would like to acknowledge the support of the Brazilian Research Agencies CNPq, CAPES and FAPERJ.

REFERENCES

Adeodato, A., Duarte, B.T., Monteiro, L.L.S., Pacheco, P.M.C.L., Savi, M.A. "Synergistic use of piezoelectric and shape memory alloy elements for vibration-based energy harvesting". International Journal of Mechanical Sciences, 194:106206, 2021.

Adeodato, A., Vignoli, L.L., Paiva, A., Monteiro, L.L.S., Pacheco, P.M.C.L., Savi, M.A. "A Shape Memory Alloy Constitutive Model with Polynomial Phase Transformation Kinetics". Shape Memory and Superelasticity, 2022.

Adeodato, A. "Synergistic use of piezoelectric and shape memory alloy elements for energy harvesting: Experimental and Numerical Analyses". Phd, CEFET/RJ 2022.

Ali, F., Raza, W., Li, X., Gul, H., Kim, K. "Piezoelectric energy harvesters for biomedical applications". Nano Energy, 19:879–902, 2019.

Dagdeviren, D., Yang, B.D., Su, Y., Tran, P.L., Joe, P., Anderson, R., Xia, J., Doraiswamy, V., Dedashti, B., Feng, X., Lu, B., Poston, R., Khalpey, Z., Ghaffari, R., Huang, Y., Slepian, J., Rogers, J.A. "Conformal piezoelectric energy harvesting and storage from motions of the heart, lung, and diaphragm". Proceedings of the National Academy of Sciences, 111(5):1927–1932, 2014.

de Aguiar, R. A. A., Savi, M. A., Pacheco, P. M. C. L. "Experimental and numerical investigations of shape memory alloy helical springs". Smart Materials and Structures, 19 (2):25008, 2010.

de Souza, C.V., de Marqui, C. "Airfoil-based piezoelectric energy harvesting by exploiting the pseudoelastic hysteresis of shape memory alloy springs". Journal of Intelligent Material Systems and Structures, 24(12):125014, 2015.

Du Toit, N.E., Wardle, B.L., Kim, S. "Design considerations for mems-scale piezoelectric mechanical vibration energy harvesters". Integrated ferroelectrics, 71(1):121–160, 2005.

Elahinia, M.H. Shape Memory Alloy Actuators. Wiley, 2016.

Enemark, S., Savi, M. A. , Santos, I. F. "Nonlinear dynamics of a pseudoelastic shape memory alloy system — theory and experiment". Smart Materials and Structures, 23(8): 085018, 2014.

Erturk, A. "Electromechanical Modeling of Piezoelectric Energy Harvesters". PhD thesis, Virginia Polytechnic Institute and State University, 2009.

Erturk, A. and Inman, D. J. Piezoelectric Energy Harvesting. John Wiley - Sons, Inc, 2011.

Lagoudas, D. Shape Memory Alloys. Springer, 2008.

Lee, H.J., Sherrit, S., Tosi, L.P., Walkemeyer, P., Colonius, T. "Piezoelectric energy harvesting in internal fluid flow". Sensors, 15(10):26039–26062, 2015.

Leo, D.J. "Engineering Analysis of Smart Materials and Structures". John Wiley and Sons, Inc., 2007.

Karadag, C.V., Topaloglu, N. "A self-sufficient and frequency tunable piezoelectric vibration energy harvester". Journal of Vibration and Acoustics, 139(1):11013, 2017.

Park, D.Y., Joe, D. J., Kim, D.H., Park, H., Han, J.H., Jeong, C.K., Park, H., Park, J.G., Joung, B., Lee, K.J. "Self-powered real-time arterial pulse monitoring using ultrathin epidermal piezoelectric sensors". Advanced Materials, 29(37):1702308, 2017.

Savi, M.A. "Nonlinear dynamics and chaos in shape memory alloy systems". International Journal of Non-Linear Mechanics, 70, 2015.

Sodano, H.A., Park, G., Inman, D.J. "Estimation of electric charge output for piezoelectric energy harvesting". Strain, 40(2):49–58, 2004. (a).

Sodano, H.A., Inman, D.J., Park, G. "Comparison of piezoelectric energy harvesting devices for recharging batteries".

Journal of Intelligent Material Systems and Structures, 16(10):799–807, 2005 (b).

Tran, N., Ghayesh, M.H., Arjomandi, M. ”Ambient vibration energy harvesters: A review on nonlinear techniques for performance enhancement”. International Journal of Engineering Science, 127:162–185, 2018.

Williams, C. B. and Yates, R.B. ”Analysis of a micro electric generator for microsystems”. Sensor and Actuators, a Physical, 52(1-3):8–11, 1996.

RESPONSIBILITY NOTICE

The authors are the only responsible for the printed material included in this paper.